PROCEEDINGS, 51st Workshop on Geothermal Reservoir Engineering
Stanford University, Stanford, California, February 9-11, 2026
SGP-TR-230

Coupled THMC Flow-Through Experiments and Decision Analysis of Proppant Performance under Utah FORGE EGS Conditions

Bruce Mutume[1], Ali Ettehadi[1], Terry Palisch[2], Wenming Dong[3]

[1]Hydraulic Barrier Material and Geomimicry Laboratory, School of Chemical Engineering, Oklahoma State University, 420 Engineering North, Stillwater, OK, 74078, USA
[2]CARBO Ceramics Inc, 5050 Westway Park Blvd, Houston, TX 77041, USA
3Energy Geosciences Division, Lawrence Berkeley National Laboratory, 1 Cyclotron Road, Berkeley, CA, 94720, USA
bruce.mutume@okstate.edu, ali.ettehadi@okstate.edu, terrence.palisch@carboceramics.com, wenmingdong@lbl.gov.

Keywords: EGS; Utah FORGE; Proppant Stability; THMC Testing; Ceramic Proppants; AHP Ranking.

ABSTRACT

Thermo-hydro-mechanical-chemical (THMC) flow-through experiments were conducted to evaluate the stability of three proppant systems under Utah FORGE-representative EGS conditions. Quartz sand (FORGE 40/70), Carbolite 40/70, and Kryptosphere LD (40 mesh) were confined between granitoid platens and exposed to 2,000-6,000 psi and 200 °C in deionized water. Mineralogical, chemical, and mechanical responses were assessed using XRD, SEM-EDS, ICP-MS, and API sieve analysis, and compared with earlier thermo-chemical (TC) batch tests in Utah FORGE fluids at 220 °C.

XRD shows that both ceramic proppants maintained their crystalline structure under TC and THMC loading, though with amorphous-peak changes. FORGE sand exhibited stronger feldspar-range peak modifications in FORGE fluids than in DI-water THMC tests, confirming the dominant role of fluid chemistry in dissolution pathways. SEM-EDS indicates stress-enhanced surface alteration; mainly Al-Si reactivity on ceramics and Fe removal from FORGE sand, but with limited correspondence between TC and THMC trends. ICP-MS results show that THMC conditions significantly increase dissolution relative to TC tests, with cumulative major-element release (TIRI) lowest for Kryptosphere LD (~2.6×10^5 ppb), intermediate for FORGE sand (~2.66×10^5 ppb), and highest for Carbolite (~3.12×10^5 ppb). Sieve analysis reveals negligible <140-mesh fines for the ceramics but ~22 % fines and a high conductivity-weighted breakage index (CWBI ≈ 52-55) for FORGE sand, indicating severe mechanical degradation.

A multi-criteria decision framework (AHP) integrating TIRI, CWBI, and price weighted fines most heavily (0.584), followed by price (0.281) and dissolution (0.135). Resulting scores were 0.752 (Carbolite), 0.719 (Kryptosphere LD), and 0.400 (FORGE sand), showing that mechanical integrity is the dominant factor governing performance under geothermal THMC conditions. Ceramic proppants therefore outperform sand despite higher cost. These rankings apply only to the tested materials and selected criteria; future work should incorporate additional performance metrics and expanded proppant classes.

1. INTRODUCTION

Enhanced geothermal systems (EGS) increasingly rely on engineered propped fractures to sustain high-permeability flow paths between injection and production wells. Unlike conventional hydrothermal systems, where natural fractures may support production, EGS stimulation typically requires placement of mechanically competent proppants to prevent premature fracture closure under high confining stress and elevated temperatures. Proppant-supported fracture networks therefore play a critical role in maintaining long-term hydraulic conductivity and enabling durable heat extraction within crystalline reservoirs.

Field demonstrations have shown that proppant-assisted stimulation can dramatically enhance geothermal performance. Early German projects reported up to fifteen-fold production increases (Zimmermann et al., 2008), while recent developments at Utah FORGE (McLennan et al., 2023) and commercial pilots by Fervo Energy (Fercho et al., 2023) validate operational scalability. The Mazama Energy super-hot EGS test further demonstrated the feasibility of deploying advanced ceramic proppants in reservoirs approaching ~330 °C and elevated pressures (CARBO, 2025), reinforcing the potential role of engineered proppants in next-generation geothermal systems. However, these successes also highlight unresolved challenges associated with deploying proppants originally designed for oil and gas environments into far more extreme geothermal conditions. Most commercial proppants; natural sand and resin-coated composites, were engineered for service temperatures below ~120 °C (Nadeau et al., 2023) and for chemically moderate formation waters. While ceramic proppants enabled stimulation of higher-temperature wells (up to ~175 °C) relative to sand-based systems, they were not explicitly engineered for prolonged exposure to the extreme temperatures, chemically aggressive fluids, and long residence times characteristic of enhanced geothermal systems. In contrast, EGS environments expose proppants to 200-220 °C, dynamic fluid-rock interaction, evolving pH, and long-term flow-through exposure lasting years to decades. Time-series analyses at Utah FORGE show that injected fluids undergo rapid geochemical evolution due to feldspar dissolution, amorphous silica precipitation, and alkaline cation release (Simmons et al., 2025). Such conditions can accelerate proppant dissolution, induce fines generation, and promote secondary mineral precipitation that degrades fracture conductivity. Consequently, proppant selection for geothermal applications must consider full thermo-hydro-mechanical-chemical (THMC) compatibility rather than relying solely on criteria developed for oil and gas operations. The Utah Frontier Observatory for Research in Geothermal Energy (FORGE) offers an ideal natural laboratory for assessing these issues. The reservoir consists of high-temperature granitoids north of Milford, Utah (Jones et al., 2024), with injection well 16A(78)-32 exhibiting ~219 °C bottom-hole temperature at 3274 m and minimum horizontal stresses near 4500 psi (Mcclure, 2025). Recent stimulations employed slickwater and CMHPG fluids with microproppant additions to establish connectivity between 16A and 16B (McLennan et al., 2023), providing a realistic

basis for laboratory replication of reservoir conditions. Despite these advances, significant gaps persist in understanding proppant degradation pathways under fully coupled THMC loading. Prior geothermal studies often relied on short-duration or static batch tests that do not capture pressure-driven dissolution, fines mobilization, or microstructural abrasion within active fracture networks. As EGS development progresses toward deeper, hotter, and more chemically reactive reservoirs, there is a pressing need for data-driven frameworks that quantitatively evaluate proppant performance and translate laboratory behavior into actionable selection criteria.

This study addresses these gaps by evaluating the THMC stability of three representative proppant types; FORGE 40/70 sand, a premium low-density ceramic (40/70), and an advanced ultra-conductive ceramic (40) using a continuous flow-through system at 200 °C and 2,000-6,000 psi. We quantify mineralogical stability (XRD), surface alteration (SEM-EDS), elemental dissolution (ICP-MS), and particle-size redistribution (API sieve analysis). These experimental results are synthesized using a multi-criteria decision-making (MCDM) framework based on the Analytic Hierarchy Process (AHP), using three geothermal-relevant criteria: price, fines generation, and dissolution. By integrating THMC experimentation with structured decision analysis, this work provides a robust and scalable framework for selecting proppants tailored to high-temperature geothermal environments. The findings support the engineering and deployment of more durable proppant systems as the geothermal industry advances toward deeper and hotter EGS reservoirs. This study is intended to stimulate discussion on how laboratory-scale THMC flow-through testing can be translated into practical, comparative proppant screening tools for enhanced geothermal systems.

2. EXPERIMENTAL MATERIALS AND RATIONALE

The experimental workflow (Figure 1) was designed to evaluate proppant suitability for geothermal deployment based on three decision criteria: price, fines generation, and dissolution behavior, which form the core of the AHP ranking framework used in this study. Proppants were selected to represent both field-relevant and commercial alternatives, including FORGE 40/70 sand used in the 2024 stimulation and two ceramic benchmarks (Premium Low-Density Ceramic 40/70 and Advanced Ultra-Conductive Ceramic 40 mesh). This combination ensured direct comparison between low-cost natural proppants and higher-performance engineered ceramics under identical THMC conditions. Modified API 19D flow-through testing was performed on the samples at 2000-psi, 4500-psi, and 6000-psi closure stress levels. The test was performed at a temperature of 200 °C using de-ionized water solution. The cells are loaded at 2lb/ft^2 between reservoir granite obtained from the Utah FORGE 16B-78(32) well at a depth of 9,842.2-9,843.0 ft. This methodology simulates progressive fracture closure under realistic thermal and mechanical conditions to quantify fines generation and dissolution. Post-test analyses using SEM-EDS, XRD, ICP-MS, and API sieve methods captured surface alteration, mineralogical stability, elemental release, and particle-size changes. Economic cost, fines content, and cumulative ion release were then integrated using an AHP framework to produce an objective, multi-criteria proppant ranking that balances mechanical performance, geochemical stability, and economic viability under Utah FORGE-relevant THMC conditions.

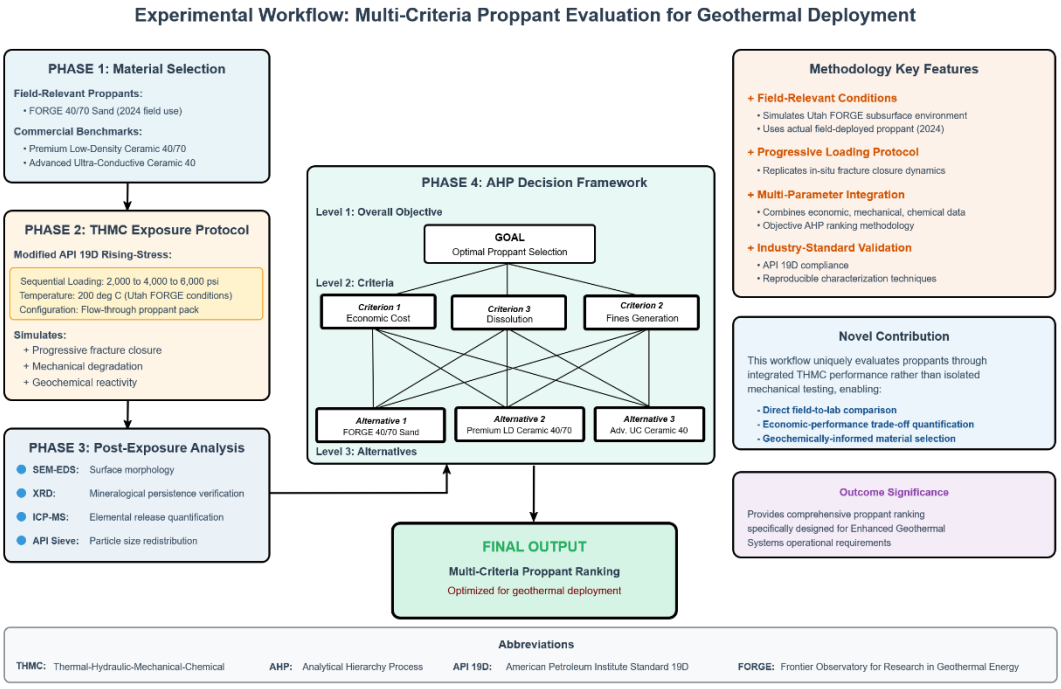

Figure 1. Three-phase methodology showing material selection, staged THMC loading using a modified API 19D protocol, and post-characterization of reacted proppants.

2.1 AHP Weighting Procedure (Saaty Method)

The Analytic Hierarchy Process (AHP) is a widely used multi-criteria decision-making method applied across many fields, including power plant siting (Mutume, 2023), agriculture, and infrastructure planning. In this study, AHP was used to derive expert-based weights

for the three key proppant selection criteria: dissolution, fines generation, and price. Criterion weighting followed the classical Saaty method (Saaty & Vargas, 1979), using pairwise comparisons to establish relative importance. The procedure followed the classical Saaty method and consisted of the following steps:

1. Define the decision hierarchy, with the overall goal (most robust proppant selection under tested conditions) at the top level, followed by the three criteria, and the proppant alternatives at the lower level.

2. Construct the pairwise comparison matrix $A = a_{ij}$ for the criteria, where each element a_{ij} represents the relative importance of criterion i over criterion j using Saaty's 1-9 scale. Reciprocal values were assigned as $a_{ji} = {}^{1}/_{a_{ij}}$.

3. Compute the priority vector (criteria weights) by calculating the normalized principal eigenvector of matrix AAA. For the 3×3 matrix in this study, the dominant eigenvalue λ_{max} was obtained from:

   a. $\lambda_{max} = \sum_{j=1}^{n} \cdot \left(\sum_{i=1}^{n} a_{ij} w_i\right)$ (1)

and the corresponding eigenvector was normalized to yield the weight vector w.

4. Evaluate consistency of expert judgments using the Consistency Index CI and Consistency Ratio CR:

   a. $CI = \frac{\lambda_{max} - n}{n-1}$ (2)

   b. $CR = \frac{CI}{RI}$ (3)

5. where $n = 3$ is the number of criteria and RI is Saaty's Random Index. A $CR < 0.10$ indicates acceptable consistency.

6. Construct the normalized decision matrix by applying linear normalization to the performance values for each criterion, ensuring that lower values of dissolution, fines generation, and price obtain higher scores.

7. Compute the final AHP score for each proppant using a weighted sum model:

   a. $S_i = \sum_{j=1}^{n} w_j x_{ij}$ (4)

where x_{ij} is the normalized performance of proppant iii under criterion j.

The AHP is applied here as a structured decision-support framework to organize discussion across multiple performance metrics rather than as an optimization model. Weighting factors reflect project-specific priorities and experimental objectives and are not intended to represent universal or field-wide preferences.

2.2 Characterization Techniques

Mineralogical changes in pristine and reacted proppants were evaluated using a Bruker D8 Advance X-ray diffractometer (3-80° 2θ). High-resolution scans enabled detection of peak shifts, amorphous-phase development, and dissolution- or recrystallization-related transformations. Mineral phases were identified using DIFFRAC.SUITE EVA.

Surface morphology and microchemical alteration were assessed using a FEI Quanta 600 FEG Environmental SEM coupled with Bruker EDS. Iridium-coated grains were imaged to document abrasion features, microfractures, deposition layers, and surface enrichment patterns. EDS point spectra and area maps provided qualitative assessment of element redistribution associated with TC and THMC exposure.

Dissolved elemental concentrations in effluent fluids were measured using an Agilent 8900 Triple Quadrupole ICP-MS (ICP-QQQ) to quantify mobilization of Si, Al, Fe, Ca, Mg, trace metals, and other species indicative of proppant or rock dissolution. Sample preparation followed strict clean-lab protocols: all fluids were acidified to 2% ultrapure HNO_3 (v/v) using 18.2 MΩ·cm Milli-Q water, then filtered and diluted according to expected analyte concentrations. Instrument calibration, collision/reaction cell tuning, and QC/QA validation were conducted following established methods (Belkouteb et al., 2023) and (*Handbook of ICP-QQQ Applications*, 2012). Internal standards, duplicate analyses, calibration verification standards, and reagent blanks were incorporated to ensure analytical accuracy, stability, and reproducibility across the full 150-h experiment. A Total Ion Release Indicator (TIRI), herein referred to as a relative ion release indicator (TIRI), was used to compare cumulative dissolved ion release across proppant systems. TIRI is not mass-normalized and does not represent a dissolution rate; rather, it is used as a comparative indicator of chemical reactivity under identical THMC exposure conditions.

Mechanical degradation was assessed using API-compliant sieve analysis to quantify particle-size redistribution and <140-mesh fines generated under coupled THMC loading. These results were synthesized into a Conductivity-Weighted Breakage Index (CWBI), a screening metric designed to compare relative fines sensitivity under identical conditions, with weighting factors focused on conductivity-relevant fines generation rather than absolute conductivity loss.

3. RESULTS

The results integrate mineralogical and microstructural responses of the three proppant systems under fully coupled THMC conditions and compare them with prior decoupled thermo-chemical (TC) hydrothermal experiments conducted in Utah FORGE fluids at 220 °C (Mutume et al., 2025). This comparative framework highlights the importance of using geothermal-specific chemistries and pressure-temperature trajectories when evaluating proppant stability, as DI-water-based tests may under- or over-estimate reactivity, dissolution, or amorphous-phase formation.

3.1 XRD Results

XRD patterns of pristine, TC-exposed, and THMC-reacted proppants (Figure 2) were evaluated to track mineralogical persistence and identify reaction-induced changes through peak appearance/disappearance, 2θ shifts, and relative intensity variations. These metrics reflect dissolution-precipitation processes, cation exchange, and structural reorganization, acknowledging that amorphous or nanocrystalline products may fall below XRD's ~2 wt.% detection limit. For Carbolite and Kryptosphere LD, TC exposure in FORGE fluids suppressed the broad amorphous hump observed in pristine materials, indicating partial reorganization or removal of those phases, whereas DI-based THMC tests retained or enhanced amorphous scattering.

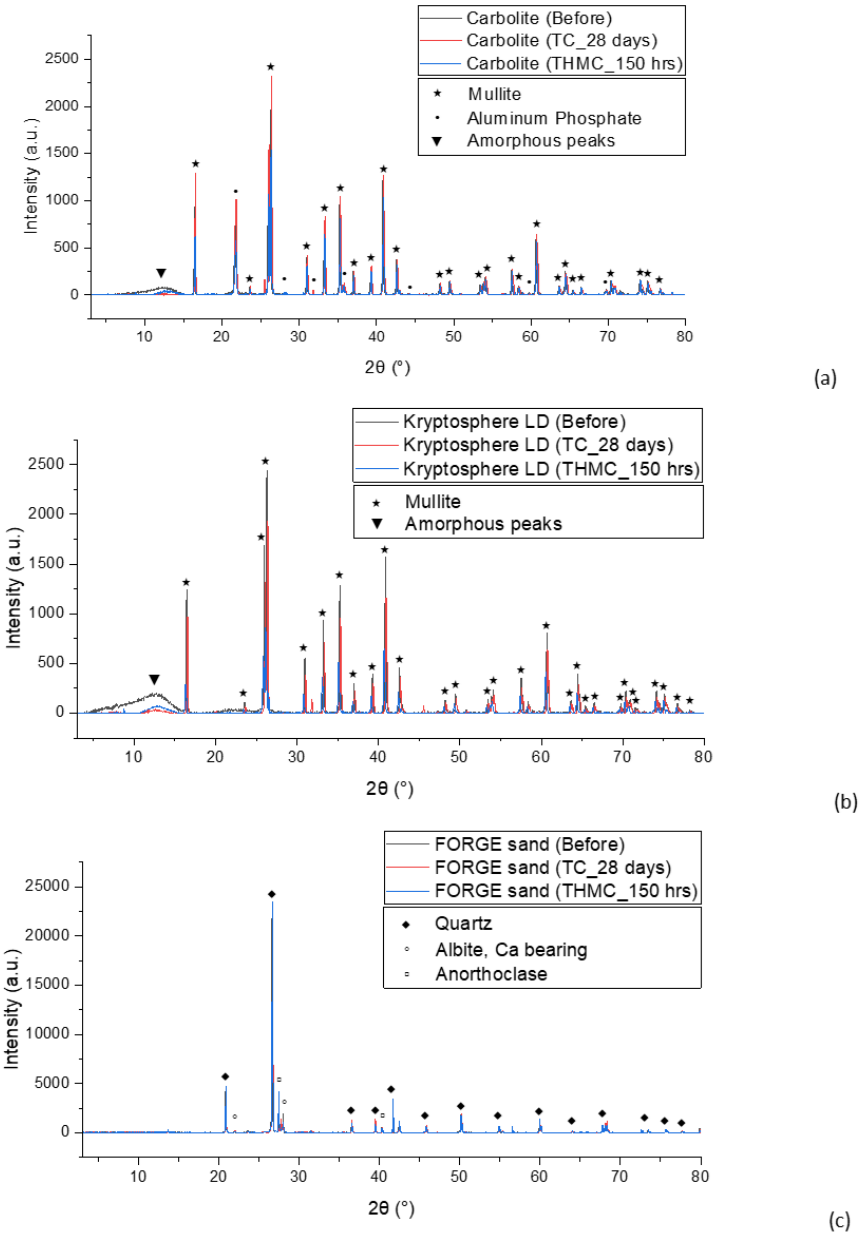

Figure 2. XRD diffractograms for (a) Carbolite, (b) Kryptosphere LD, and (c) FORGE sand comparing pristine materials (black), TC exposure in FORGE fluids at 220 °C (red), and DI-water THMC exposure at 200 °C (blue).

FORGE sand showed its most reactive region between 25°-30° 2θ, corresponding to the albite–plagioclase feldspar range. TC exposure in FORGE fluids produced clear shifts and intensity changes consistent with feldspar dissolution and Na-Ca exchange, while DI-THMC conditions produced weaker or inconsistent responses. Collectively, these results confirm that fluid chemistry exerts primary control over mineral alteration pathways and underscore the need for geothermal-specific media when evaluating proppant stability.

3.2 SEM-EDS Results

SEM micrographs (Figure 3) show clear contrasts in the surface response of the three proppants under pristine, TC, and THMC conditions. TC exposure at 220 °C produced only limited alteration for all materials; minor patchy deposits, slight edge rounding, and weak surface texturing, consistent with chemically driven modification under static hydrothermal conditions. In contrast, THMC loading at 200 °C and 2,000-6,000 psi induced more pronounced abrasion features, localized microfractures, and surface-scale material redistribution associated with grain-to-grain contact and mechanical confinement.

Although SEM images show visible crushing features in the ceramic proppants, sieve analysis confirms that these breakage events did not generate fines (<140 mesh); instead, fragmentation remained within primary mesh classes. Kryptosphere LD maintained the most intact surface morphology, whereas Carbolite exhibited slightly more abrasion and chipping. FORGE sand, by comparison, developed angular micro-fractures and fragment detachment consistent with brittle quartz failure, which correlates with the fines observed in its sieve distribution.

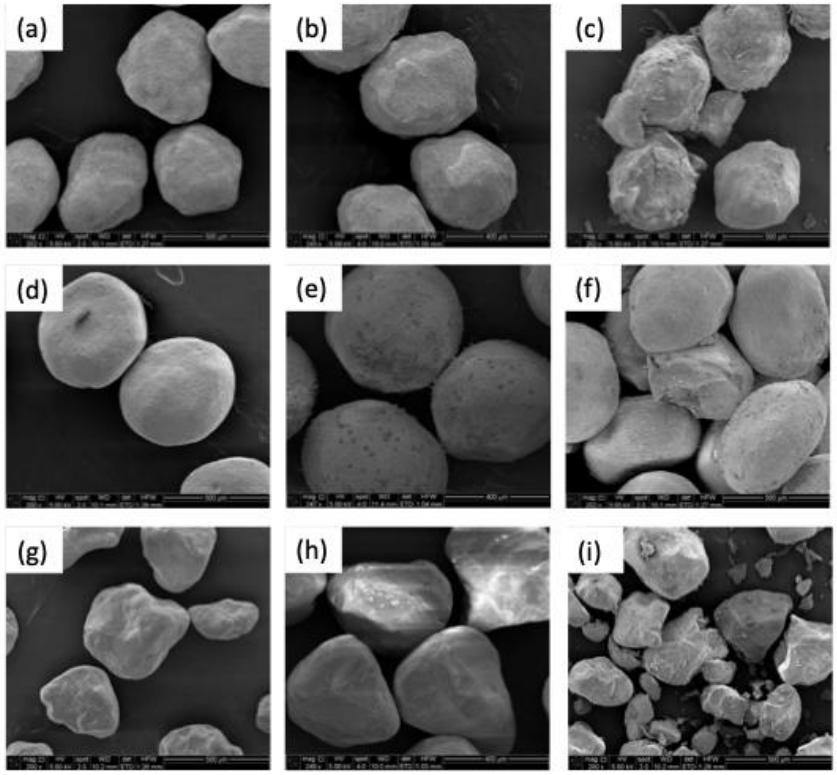

Figure 3. Representative SEM micrographs of Carbolite (a-c), Kryptosphere LD (d-f), and FORGE sand (g-i) showing (a, d, g) pristine grain surfaces prior to exposure, (b, e, h) post-thermo-chemical (TC) exposure in Utah FORGE geothermal fluids at 220 °C, and (c, f, i) post-THMC flow-through loading at 200 °C and 2,000-6,000 psi. Images highlight differences in surface roughening, microfracturing, and particle-edge abrasion, with ceramic proppants exhibiting minimal mechanical damage and no fines detachment, while FORGE sand shows angular fragmentation consistent with brittle quartz failure.

SEM-EDS spectra (Table 1) reveal surface-level compositional shifts across aluminum, silicon, phosphorus, and iron after TC and THMC exposure, indicating dissolution, surface enrichment, and mechanically assisted alteration. THMC loading produced the clearest signatures of stress-enhanced reactivity, including stronger Al depletion in Carbolite (-45%), Fe removal in FORGE sand (-18%), and mixed gains and losses associated with abrasion and reprecipitation. In contrast, TC results did not consistently align with THMC outcomes; some trends were amplified under TC (e.g., larger Al loss in sand and Kryptosphere), while others reversed direction (e.g., P enrichment under THMC vs. slight losses under TC). This lack of systematic correspondence demonstrates that SEM-EDS alone cannot be used to quantify the degree of proppant reactivity.

Because SEM-EDS captures only localized surface chemistry rather than bulk mineralogical change or the composition of liberated fragments, the percent changes represent qualitative indicators of reaction pathways rather than measures of total degradation. These

patterns therefore confirm active fluid-solid interaction under both TC and THMC conditions, but must be interpreted alongside XRD, ICP-MS, and sieve analysis to evaluate overall proppant stability under EGS-relevant THMC conditions.

Table 1: Percent change in elemental surface composition of Carbolite, Kryptosphere LD, and FORGE sand after thermo-chemical (TC) and fully coupled THMC exposure, normalized to pristine values. "NP" indicates appearance of a new detectable phase where the element was absent before exposure. Values represent qualitative indicators of surface alteration rather than bulk reactivity, reflecting the limitations of SEM-EDS as a localized surface probe.

Element	Carbolite		Kryptosphere LD		FORGE Sand	
	TC	THMC	TC	THMC	TC	THMC
Na	0.0%	0.0%	NP	0.0%	-47.4%	-43.9%
Mg	0.0%	0.0%	NP	0.0%	NP	0.0%
Al	-23.2%	-45.3%	-55.8%	-14.7%	-77.4%	-4.0%
Si	+2.0%	+11.2%	+37.1%	-17.4%	+18.3%	+7.3%
P	+42.3%	+60.1%	-13.6%	+26.4%	-2.8%	+30.9%
Ca	NP	0.0%	NP	0.0%	NP	0.0%
Fe	0.0%	NP	+120.7%	+6.3%	-98.3%	-18.2%

3.3 ICP-MS Results

Table 2 presents the starting-fluid chemistry and effluent concentrations for both TC and THMC experiments, along with the corresponding percent changes.

Table 1. ICP-MS concentrations of major dissolved elements in starting fluids and effluents from the thermo-chemical (TC) and fully coupled THMC experiments. Values allow direct comparison of element release under chemically driven TC conditions and mechanically enhanced THMC conditions. Percent-change calculations referenced in the text are based on normalization to the respective starting fluids for each test.

Material / Fluid	Si	Al	P	Ca	Fe	Na	Mg
TC Starting Fluid (Utah FORGE Fluid Before)	67,824.35	31.71	611.30	187,118.55	53.31	2,436,624.05	11,315.84
TC Effluent-Kryptosphere	102,098.94	15.55	233.43	159,883.38	32.92	2,330,881.96	173.15
TC Effluent-FORGE Sand	110,077.24	192.07	225.60	150,634.65	N.D	2,383,544.92	589.75
TC Effluent-Carbolite	98,870.16	65.53	207.16	153,336.99	N.D	2,376,567.19	319.31
THMC Starting Fluid (DI Water Before)	1,105.70	N.D	101.99	344.35	N.D	2,967.17	N.D
THMC Effluent - Kryptosphere	68,619.19	6,744.10	N.D	7,359.14	104.15	180,339.10	542.23
THMC Effluent - FORGE Sand	86,796.49	3,086.83	N.D	3,550.62	23.12	177,022.44	330.14
THMC Effluent - Carbolite	136,759.81	6,046.54	16.51	3,789.62	31.90	169,644.05	303.57

* Concentrations in ppb. N.D = Non-Detectable.

Normalizing TC effluents to the FORGE fluid baseline shows modest hydrothermal alteration, with silicon increasing by 50-62 %, phosphorus decreasing by over 60 %, and magnesium decreasing by more than 95 % across all proppants. Aluminium behavior varied strongly, ranging from a 51 % decrease for Kryptosphere to a 506 % increase for FORGE sand. In contrast, THMC conditions produced much larger shifts when normalized to DI water, with silicon increasing by 6,107-12,267 %, calcium by 932-2,036 %, and sodium by 5,600-6,000 %, while phosphorus was fully removed and aluminium and iron appeared despite being undetectable in the starting fluid.

These trends demonstrate that TC tests capture limited hydrothermal leaching, whereas THMC loading amplifies dissolution and ion exchange by more than an order of magnitude. Based on the total ions released, Kryptosphere LD exhibited the lowest cumulative ion release (~2.6×10^5 ppb), indicating the highest chemical stability under THMC conditions. FORGE sand showed intermediate reactivity (~2.66×10^5 ppb), while Carbolite released the largest dissolved-ion load (~3.12×10^5 ppb), consistent with stronger stress-assisted dissolution. These results confirm that mechanical loading not only increases dissolution rates but also differentiates proppant chemical stability in a way not captured by TC tests alone.

3.4 Sieve Results

Sieve analysis before and after THMC exposure shows that Kryptosphere LD underwent only minor redistribution, with the main 40-mesh class decreasing from 89.4 % to 82.7 % and a modest increase in the 35-mesh fraction from 2.5 % to 14.8 %, while no fines (<140 mesh) were generated. Carbolite showed similarly limited degradation, with its primary 45-mesh mode decreasing only slightly from 73.7 % to 71.3 % and small changes occurring in the adjacent 35-70 mesh classes, again with no fines production. In contrast, FORGE sand exhibited substantial mechanical breakdown, with the 45-mesh peak collapsing from 73.7 % to 7.1 % and material redistributing across finer classes down to the pan. Approximately 22 % of the sand mass entered the <140-mesh fines region, indicating extensive grain crushing and high fines mobility potential. According to API RP 19C criteria, this level of fines generation is expected to significantly reduce proppant-pack conductivity under reservoir loading.

3.4.1 Conductivity-Weighted Breakage Index (CWBI)

Mechanical degradation was quantified using a conductivity-weighted breakage index (CWBI), which measures the mass shifting into finer sieve classes that are known to impair fracture conductivity in API 19C testing. Only downward transitions are penalized, and each sieve class is weighted according to the hydraulic severity of fines generation. This produces a compact, conductivity-aligned measure of proppant stability under THMC exposure. The index is computed as:

$$CWBI = \sum w_i \times \Delta P_{i(finer)} \quad (5)$$

Where, $\Delta P_{i(finer)}$, is the downward shift into finer size classes, defined as $\Delta P_{i(finer)} = Max(P_{i(after)} - P_{i(before)})$ and w_i is the conductivity-severity weight for each mesh interval. The weighting scheme used in this study is: 35-45 mesh = 0.1; 50-60 mesh = 0.3; 70-100 mesh = 0.6; <140 mesh and pan = 1.0. The key sieve-based degradation metrics and the corresponding conductivity-weighted breakage index (CWBI) values for the three proppants are summarized in Table 3.

Table 3. Sieve-Based Degradation Metrics and CWBI Values.

Proppant	Fines (<140 mesh) (%)	Primary Mode Before	Primary Mode After (%)	Primary Mode Loss (%)	CWBI
Kryptosphere LD	0	40mesh=89.4%	82.7	6.7	0.5-0.8
Carbolite	0	45mesh=73.7%	71.3	2.4	0.7-1.0
FORGE sand	~22	45mesh=73.7	7.1	66.6	52-55

3.5 MCDM-AHP Results

A multi-criteria decision-making assessment using the Analytic Hierarchy Process (AHP) was conducted to integrate dissolution (TIRI), fines generation (CWBI), and price into a single comparative performance metric for the three proppants. The resulting consistency ratio (CR = 0.117) is slightly above the 0.10 threshold required for strict AHP consistency, exceeding it by only 0.017; this deviation is small and indicates that expert judgments are reasonably coherent, though not perfectly consistent. Linear normalization (lower = better) was applied to all quantitative inputs. As shown in Table 4, both ceramic proppants exhibited excellent fines resistance, while FORGE sand displayed substantially higher degradation. Kryptosphere LD showed the lowest dissolution values, whereas Carbolite benefited from a significantly lower cost. When weighted by the expert-derived criteria importance, Carbolite achieved the highest overall AHP score (0.752), followed closely by Kryptosphere LD (0.719). FORGE sand ranked last (0.400), driven primarily by fines-related penalties despite its favorable price. Overall, the AHP results confirm that mechanical stability is the dominant driver of proppant suitability under geothermal THMC conditions, and that ceramic proppants provide superior performance relative to sand, with cost differences influencing the ranking within ceramic classes.

These results highlight the importance of balancing technical performance with economic considerations when selecting proppants for geothermal applications. A cost-only assessment would favor FORGE sand despite its poor mechanical performance under THMC conditions, whereas a strength-only perspective would prioritize Kryptosphere LD due to its superior fines resistance. By integrating dissolution behavior, mechanical stability, and price within a single MCDM framework, the AHP analysis identifies Carbolite as the most preferred within this experimental scope, offering substantially improved THMC performance relative to sand while providing a more favorable cost-performance balance than Kryptosphere LD. This outcome underscores the value of multi-criteria decision tools for guiding proppant selection in EGS deployments, where neither cost nor technical metrics alone are sufficient.

Table 4. Inputs, normalized performance values, AHP criteria weights, and final ranking of the three evaluated proppants. The table integrates dissolution (TIRI), fines generation (CWBI), and price metrics using linear normalization and Saaty-derived criterion weights to produce the final AHP decision scores.

Parameter	Kryptosphere LD	Carbolite	FORGE sand
Raw Inputs			
TIRI (ppb)	2.60×10^5	3.12×10^5	2.66×10^5
CWBI (fines)	0.65	0.85	53.5
Price ($/lb)	0.60	0.30	0.10
Normalized Score			
Dissolution	1.000	0.000	0.885
Fines	1.000	0.998	0.000
Price	0.000	0.600	1.000
AHP Weights	0.135	0.584	0.281
Final AHP Score	0.719	0.752	0.400
Rank	**2**	**1**	**3**

4. CONCLUSIONS AND RECOMMENDATIONS

THMC flow-through experiments conducted at 200 °C and 2,000-6,000 psi revealed clear mineralogical, chemical, and mechanical stability differences among the tested proppants. Both ceramic systems; Carbolite and Kryptosphere LD, maintained their crystalline structure under TC and THMC exposure, exhibiting only minor amorphous-phase evolution. In contrast, FORGE sand showed pronounced feldspar-range peak modifications, particularly in FORGE-fluid TC tests, indicating a stronger sensitivity to fluid chemistry and greater potential for framework alteration under true geothermal reservoir conditions.

Chemical analyses further demonstrated that THMC conditions substantially increased dissolution relative to TC tests. Kryptosphere LD produced the lowest cumulative dissolved-ion release (TIRI ≈ 2.6×10^5 ppb), followed closely by FORGE sand (≈ 2.66×10^5 ppb), while Carbolite generated the highest TIRI (≈ 3.12×10^5 ppb) despite retaining structural integrity. SEM–EDS revealed active surface alteration across all samples, characterized by Al-Si adjustments on ceramic grains and notable Fe depletion on FORGE sand. However, the lack of systematic correspondence between TC and THMC reactivity trends, combined with the use of different fluids in the two tests, underscores the limited ability of SEM-EDS to serve as a standalone indicator of bulk degradation.

Mechanical stability emerged as the dominant factor governing proppant performance. Sieve analysis showed negligible <140-mesh fines for both ceramic proppants, whereas FORGE sand produced ~22% fines and exhibited a high CWBI (≈ 52-55), indicating severe crushing and a strong likelihood of conductivity loss under reservoir stresses. When incorporated into the AHP decision framework, this mechanical failure mode overwhelmingly influenced overall suitability. Expert weighting prioritized fines generation (0.584) over price (0.281) and dissolution (0.135), resulting in scores of 0.752 for Carbolite, 0.719 for Kryptosphere LD, and 0.400 for FORGE sand. The AHP framework is intended to support engineering judgment rather than produce a unique or universally optimal ranking.

The primary contribution of this study lies not in identifying a single ‘best’ proppant, but in demonstrating a workflow for integrating thermo-hydro-mechanical-chemical flow-through testing with multi-criteria decision analysis. The study shows how chemical dissolution, mechanical degradation, and economic considerations, often reported independently, can be evaluated jointly within a transparent engineering framework. Importantly, this framework is extensible and can incorporate additional datasets, performance metrics, or project-specific priorities as future experimental or field data become available.

Recommendations:

The integrated THMC, mineralogical, and decision-analysis results strongly support the use of ceramic proppants in high-temperature EGS environments where long-term fracture conductivity is essential. Although FORGE sand demonstrates moderate chemical stability, its significant fines generation under FORGE-representative stresses makes it unsuitable for sustained geothermal operations. Given the higher cost of ceramics, future research should investigate geothermal-specific enhancements technologies (such as coatings, etc) as a pathway to improving the performance of sand proppants while keeping overall material cost low. Additional testing could incorporate thermal cycling, silica-scaling tendencies, coating durability, and extended-duration flow-through experiments, including evaluations of coated, graphene-enhanced, and nanoparticle-reinforced proppants. Coupling these experimental results with reservoir-scale simulations will further refine proppant design and enable site-specific selection tailored to geothermal THMC conditions.

Acknowledgements

This material is based upon work supported by the U.S. Department of Energy, Geothermal Technologies Office, under Award Number DE-EE0007080 for the Enhanced Geothermal System Concept Testing and Development at the Milford City, Utah FORGE Site, and under Contract UEI Number NNYDFK5FTSX9, Project Number 9-3706. Parts of this work were carried out in the Microscopy Laboratory at Oklahoma State University, which received funding for equipment from the NSF MRI program. We are grateful to the Utah FORGE team for providing rock, proppant and fluid samples. We also thank CARBO Ceramics for supplying the proppant materials used in this study. The author gratefully acknowledges Dr. Mileva Radonjic for her foundational role in initiating and conceptualizing this project, for her guidance in defining the research direction, and for serving as the Principal Investigator who secured the funding that made this work possible. Special thanks to the OSU Geomimicry Group for their valuable support throughout this work. Their generous support and collaboration were invaluable to the success of this research.

REFERENCES

Belkouteb, N., Schroeder, H., Arndt, J., Wiederhold, J. G., Ternes, T. A., & Duester, L. (2023). Quantification of 68 elements in river water monitoring samples in single-run measurements. *Chemosphere*, *320*, 138053. https://doi.org/10.1016/j.chemosphere.2023.138053

CARBO. (2025, November 5). Mazama Energy Completes the World's Hottest Enhanced Geothermal System. *Carbo Ceramics*. https://carbo.tech/newsroom/mazama-energy-completes-worlds-hottest/

Fercho, S., Norbeck, J., Mcconville, E., Hinz, N., Wallis, I., Titov, A., Agarwal, S., Dadi, S., Gradl, C., Baca, H., Eddy, E., Lang, C., Voller, K., & Latimer, T. (2023). *Geology, State of Stress, and Heat in Place for a Horizontal Well Geothermal Development Project at Blue Mountain, Nevada*.

Handbook of ICP-QQQ applications. (2012).

Jones, C., Simmons, S., & Moore, J. (2024). Geology of the Utah Frontier Observatory for Research in Geothermal Energy (FORGE) Enhanced Geothermal System (EGS) Site. *Geothermics*, *122*, 103054. https://doi.org/10.1016/j.geothermics.2024.103054

Mcclure, M. (2025). *Preliminary Analysis of Results from the Utah FORGE Project*.

McLennan, J., England, K., Rose, P., Moore, J., & Barker, B. (2023, January 24). *Stimulation of a High-Temperature Granitic Reservoir at the Utah FORGE Site*. SPE Hydraulic Fracturing Technology Conference and Exhibition. https://doi.org/10.2118/212346-MS

Mutume, B. (2023). A feasibility assessment of utilizing concentrated solar power (CSP) in the Zimbabwean regions of Hwange and Lupane. *Heliyon*, *9*(7). https://doi.org/10.1016/j.heliyon.2023.e18210

Mutume, B., Ettehadi, A., Dhanapala, B. D., Palisch, T., & Mileva, R. (2025). Geochemical Reactivity and Alteration Mechanisms of Proppant Materials in Enhanced Geothermal Systems. *Geothermal Resources Council Transactions*, *49*, 1172–1190. https://www.geothermal-library.org/index.php?mode=pubs&action=view&record=1035293

Nadeau, P. H., Sun, S., & Ehrenberg, S. N. (2023). The "Golden Zone" temperature distribution of oil and gas occurrence examined using a global empirical database. *Marine and Petroleum Geology*, *158*, 106507. https://doi.org/10.1016/j.marpetgeo.2023.106507

Saaty, T. L., & Vargas, L. G. (1979). Estimating technological coefficients by the analytic hierarchy process. *Socio-Economic Planning Sciences*, *13*(6), 333–336. https://doi.org/10.1016/0038-0121(79)90015-6

Simmons, S., Jones, C., Rose, P., & Moore, J. (2025). *The Geochemistry of Flowback and Produced Waters at Utah FORGE and Their Implications for EGS Production*.

Zimmermann, G., Reinicke, A., Brandt, W., Blöcher, G., Milsch, H., Holl, H., Moeck, I., Schulte, T., Saadat, A., & Huenges, E. (2008). *Results of Stimulation Treatments at the Geothermal Research Wells in Groß Schönebeck, Germany*. cp. https://doi.org/10.3997/2214-4609.20147634